Numerical Schemes in FEM for Plane Strain Deformation of Incompressible Solids with Applications to EPFM

J. LANTEIGNE, P. NGUYÊN-DUY and Y. BLANCHETTE
Institut de recherche d'Hydro-Québec (IREQ), 1800 montée Ste-Julie, Varennes, Québec, Canada J0L 2P0

ABSTRACT

A finite element program for incompressible deformation was developed to obtain scalable fully plastic solutions of various flawed geometries. An automatic mesh generation scheme applicable to fracture mechanics is presented. In many respects, the method used is efficient and economic. For instance, displacements and crack parameters can be determined without the computation of the hydrostatic stress. Some examples are presented.

KEYWORDS

Finite Element Method; incompressible solids; plane strain; flawed geometries; Elastic-Plastic Fracture Mechanics.

INTRODUCTION

The use of EPFM (Elastic-Plastic Fracture Mechanics) to assure structural integrity may result in structural designs where material's full plasticity capabilities can be accounted for. This can be a significant gain over LEFM especially in the case of very ductile materials.

The estimation procedure in an engineering approach proposed by Kumar and his collaborators (1981a) consists in combining elastic and fully plastic solutions by a suitable interpolation between these two extreme cases for a given applied load. Plastic solutions are given by scalable FEM solutions in the fully plastic regime while elastic solutions are given by LEFM.

As clearly demonstrated by Kumar and co-workers (1981b), Goldman and Hutchison (1975) and others, one of the advantages of assuming full material incompressibility by using power-law constitutive stress-strain relations is that a few FEM solutions may generate scaling laws that give direct dependance of the solution on certain parameters such as applied load, material hardening index, stress-strain law governing parameters, etc.

In this paper, we present some peculiarities of our FEM program (called MREP) treating various planar and axi-symmetric flawed geometries in the plastic plane deformation and incompressible state. Non-linear elasticity (J_2 deformation theory) is used and total incompressibility is assumed for the plane strain state.

FEM FORMULATION FOR PLANE STRAIN FULLY PLASTIC SOLUTIONS

The inclusion of incompressibility constraints in the admissible displacement field by direct elimination of nodal variables presents a definite advantage over other methods like the penalty function procedure (Zienkiewicz, 1977a) in which total incompressibility is only a limiting case or an upper bound solution for $\nu \to \frac{1}{2}$, or like the Lagrange Multipliers Method (Zienkiewicz, 1977b) in which the total number of nodal unknowns is increased by the hydrostatic stress. Furthermore, introducing the hydrostatic stress into the variational equation of equilibrium requires the solution of a complete set of hydrostatic stresses at each iteration of the solution process.

However, imposing the incompressibility constraints directly in the displacement variations formulation by using static condensation of nodal degrees of freedom increases considerably the bandwith of the assembled overall rigidity matrix, and therefore increases as much the computation time.

In the absence of body forces, the application of the principle of virtual work for an incompressible material leads to:

$$\int_A (S_1\delta\varepsilon_1 + S_2\delta\varepsilon_2 + S_3\delta\varepsilon_3)\, dA = \int_s (T_1\delta u + T_2\delta v)\, ds \qquad (1)$$

where A is the plane under deformation, s, the boundary on which traction T_i is applied, S_i are the deviatoric, ε_i, the strain components given as $\varepsilon_1 = \partial u/\partial x$, $\varepsilon_2 = \partial v/\partial y$ and $\varepsilon_3 = (\partial u/\partial y + \partial v/\partial x)$, and δu, δv, the displacement increment vector. In Eq. (1), all displacements satisfy the incompressibility constraint:

$$\delta\varepsilon_1 + \delta\varepsilon_2 = 0 \qquad (2)$$

In FEM, a discretized form of Eq. (1) can be written:

$$\{\delta u_i\}^T \left(\int_A [B]^T[D][B]\, dA \;\{u_i\} - \{F_i\} \right) = 0 \qquad (3)$$

in which F_i and u_i are nodal forces and displacements, [B], the strain-shape matrix and [D] the material stiffness matrix.

For CST (constant strain triangle) elements, the incompressibility constraint, Eq. (2), is given as:

$$\sum_{i=1}^{3} (B_{1\ 2i-1}\,\delta u_i + B_{2\ 2i}\delta v_i) = 0 \qquad (4)$$

AUTOMATIC MESH GENERATION

Finite element grid for fully plastic solutions of incompressible solids cannot be constructed arbitrarily like in a plane stress problem. As shown

by Nagtegaal et al. (1974), the grid configuration should be such as to obtain the maximum "DOF/constraints" ratio. The maximum ratio (for 2-D problems) is reached for a quadrilateral basic element whose diagonals form 4 CST triangles. For this arrangement, authors have demonstrated that only 3 of 4 incompressibility constraints, Eq. (4) (one for each CST in the quadrilateral) are independent, the last one being automatically satisfied. In order to produce solutions in the entire range of "crack length/width" ratio, (a/W), the FEM grid should accomodate precisely any crack length for a given geometry. Conformal transformations were used to generate nodal coordinates (x_i, y_i) of the geometry from a cartesian map in the working space U-V. Figure 1 illustrates the transformation:

$$z = \frac{\pi}{\coth^{-1}\omega} = \frac{2\pi}{\ell n\left[\frac{\omega + 1}{\omega - 1}\right]} \qquad (5)$$

where $z = x+iy$ and $\omega = u+iv$ in complex representation. The inverse is:

$$\omega = \coth\left(\frac{\pi}{z}\right) = \frac{e^{\pi/z} + e^{-\pi/z}}{e^{\pi/z} - e^{-\pi/z}} \qquad (6)$$

The origin x=0 will eventually be the crack tip. Different selections of boundaries u_{min} and u_{max} (-1 and 1.4 in the example shown in Fig. 1) will allow for different a/W ratios, whereas different selections of v_{max} (3.5 in Fig. 1) will allow for different "length/width" ratios, L/W.

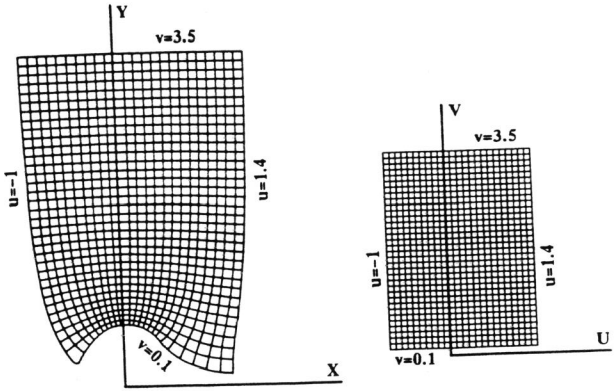

Fig. 1. Conformal mapping $z = \pi/\coth^{-1}\omega$ from space U-V to X-Y

Linear transformations such as:

$$v \leftarrow v - \Delta v\left(\frac{v_{max} - v}{v_{max} - v_{min}}\right)$$

and

$$u \leftarrow u - \Delta u\left(\frac{u_{max} - u}{u_{max} - u_{min}}\right)$$

are then used to compress the walls suitably in order to get one quarter or one half of the basic plate to be modelized. Finally, a semi-circular fine grid is adapted to the region surrounding the crack tip. Circle radii vary from the crack tip according to the geometrical progression $r_i = r_o(1.1)^i$. Typically, i = 50 and r_o = 0.002 W. Depending on boundary conditions, various geometries like single-edge or double-edge notched panel can be modelized. For axi-symmetric geometries, solid rod with penny-shaped crack or edge crack and flawed cylinders can be modelized.

STATIC NODE CONDENSATION AND CONSTRUCTION OF THE RIGIDITY MATRIX

The imposition of incompressibility constraints is done following precisely the classical analysis of Needleman and Shih (1978).

Initially, substructures consisting of two strips of N quadrilaterals are formed. In each substructure there are 6N constraints (of the type Eq. (4)) to be satisfied, i.e. 3 by quadrilateral. Of these, 4N are satisfied by eliminating the two DOF of the central node of each quadrilateral. Then, the rigidity of the substructure is obtained by combining quadrilateral element stiffness matrices. Finally, the N-1 internal nodes are condensed plus one degree of the two mid-side nodes at both extremities of the substructure. In all, this gives 6N constraints that are satisfied. The resulting reduced stiffness matrix is then (4N + 6) x (4N + 6) whereas it was initially (10N + 6) x (10N + 6). For N = 10 and 13 like substructures in Fig. 2, rigidity matrices are reduced from 106 x 106 to 46 x 46, and from 136 x 136 to 58 x 58 respectively. Therefore the total number of equations to solve is more than halved. The penalty, however, is the increased bandwith (106 as compared to 44 initially for N = 10). As shown in Fig. 2, various substructure sizes can be connected without difficulties provided global numbering of nodes is done correctly.

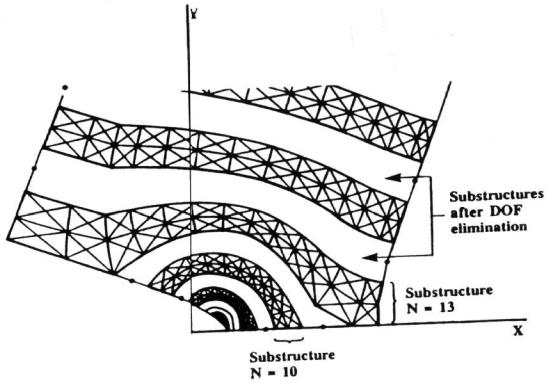

Fig. 2. Configuration of substructures in the finite element grid

The condensation of internal quadrilateral nodes uses the same scheme as for the condensation of the substructure center line of nodes, i.e. the constraint, Eq. (4) is written as:

$$[C]\ \{u_i\} = 0 \tag{7}$$

and then

$$[C_f]\{u_f\} + [C_e]\{u_e\} = 0 \tag{8}$$

in partitioned matrix notation, where $\{u_e\}$ are the nodal unknowns to be eliminated, and $\{u_f\}$, the remaining DOF. The incompressibility matrix is then formed:

$$\{u_e\} = [G]\{u_f\} \tag{9}$$

with

$$[G] = -[C_e]^{-1}[C_f] \tag{10}$$

The stiffness matrix is also partitioned as:

$$[K] = \begin{bmatrix} K_{ff} & K_{fe} \\ K_{ef} & K_{ee} \end{bmatrix}$$

and the reduced stiffness matrix, given as:

$$[K'] = [K_{ff}] + [K_{fe}][G] + [G]^T[K_{ef}] + [G]^T[K_{ee}][G] \tag{11}$$

whereas reduced element nodal forces are given as:

$$\{f'\} = \{f_f\} + [G]^T\{f_e\} \tag{12}$$

Submatrices [G] for quadrilaterals and global [G] for substructures are saved after the first computation for later use in order to recover the entire nodal parameters (displacements and residual forces) at each iteration of the solution process and to compute the hydrostatic stress once a convergent solution is obtained.

Before condensing internal nodes of quadrilaterals, care should be taken that all CST element stiffness matrices and nodal force vectors are reduced from (6 x 6) and (6 x 1) to (5 x 5) and (5 x 1) respectively.

Assembling [G], one will face the problem of inverting $[C_e]$ in Eq. (10). For all subsystems CST, quadrilaterals and substructures, $[C_e]$ is found to be a scalar, a two by two matrix and a (6N x 6N) square matrix respectively. It is a relatively small problem for most applications and standard Gaussian elimination with full pivoting technique can be used. Skyline profiled matrix can be used, but the gain will not be significant. Care should be taken however to reorganize rows of this matrix presenting a side band configuration.

ITERATIVE SOLUTION PROCESS

The global stiffness matrix and nodal force vector are obtained by assembling all substructures. Then the displacement boundary conditions are imposed and the equations solved. The Newton-Raphson method is used. For a CST, at iteration ℓ, the procedure is as follows:

Strains are obtained from the previous updated displacement vector, i.e.

$\{\varepsilon_i\} = [B]\{u_i\}^\ell$; the residual forces are computed:

$$\{R_i\}^\ell = \{P_i\} - \int_A [B]^T[D]^\ell\{\varepsilon_i\}\, dA \tag{13}$$

where $\{P_i\}$ are the applied nodal forces; a new tangent stiffness is computed, i.e. $[K_T]^\ell = \int_A [B]^T[D_T]^\ell[B]\, dA$ and $\{\Delta u_i\}^\ell$ is solved. Then the new displacements are:

$$\{u_i\}^{\ell+1} = \{u_i\}^\ell + \beta\{\Delta u_i\}^\ell \tag{14}$$

Convergence is assumed when both criteria $\|\{\Delta u_i\}^\ell\| < 0.01 \|\{u_i\}^\ell\|$ and $\|\{R_i\}\| < 0.01 \|\{P_i\}\|$ are satisfied simultaneously.

For CST elements, details of the computation are as follows: the classical 3-D constitutive stress-strain relation is used, i.e.:

$$S_i = \frac{2}{3} c\, \varepsilon_e^{(1-n)/n}\, \varepsilon_i \quad , i = 1,2$$

$$S_i = \frac{1}{3} c\, \varepsilon_e^{(1-n)/n}\, \varepsilon_i \quad , i = 3 \tag{15}$$

where ε_e, the equivalent strain is given as $\sqrt{2/3\ (\varepsilon_1^2+\varepsilon_2^2+\varepsilon_3 2/2)}$ and c is the constant $\sigma_0/(\alpha\varepsilon_0)^{1/n}$ appearing in the unidimensional law:

$$\sigma = \frac{\sigma_0}{(\alpha\varepsilon_0)^{1/n}}\, \varepsilon^{1/n}$$

The stiffness matrix [D] is then given by $(2/3\ c\varepsilon_e^{(1-n)/n}) \begin{bmatrix} 1 & 0 & 0 \\ 0 & 1 & 0 \\ 0 & 0 & \frac{1}{2} \end{bmatrix}$

The tangent stiffness matrix is given by:

$$[D_T]_{ij} = \left[\frac{\partial S_i}{\partial \varepsilon_j}\right] = \begin{bmatrix} A+B\varepsilon_1^2 & B\varepsilon_1\varepsilon_2 & B\varepsilon_1\varepsilon_3/2 \\ & A+B\varepsilon_2^2 & B\varepsilon_2\varepsilon_3/2 \\ \text{(symmetric)} & & A/2+B\varepsilon_3^2/4 \end{bmatrix} \tag{16}$$

with $A = \frac{2}{3} c\varepsilon_e^{(1-n)/n}$ and $B = \frac{4}{9} c\left(\frac{1-n}{n}\right)\varepsilon_e^{(1-3n)/n}$.

In the linear incompressible case n = 1, $[D_T]$ is reduced to [D]. Initially, a solution is found for n = 1 with arbitrary values for ε_0, α and σ_0, the material constants. The solution obtained at this value is taken as the initial starting vector for $\{u_i\}^1$ at n = 2. As a convergent solution is obtained for n = 2, say at iteration 5, $\{u_i\}^5$ is taken as the initial starting vector $\{u_i\}^1$ at n = 3, and so on. As the solution is progressing, the system becomes highly non linear, and ε_0 is adjusted to lower values to prevent divergence. For n > 5, the relaxation factor β (Eq. (14)) initially set equal to 1 is decreased to values as low as 0.2 in order to moderate the convergence rate when displacement increments become too large. Otherwise, the solution "locks" at a certain displacement without resorbing the residual force.

DETERMINATION OF CRACK PARAMETERS

The program was tested for a single-edge cracked plate (a/W = 0.6) under three-point bending. For comparison purposes with the earlier work of Kumar and co-workers (1981b), the same normalization (per unit thickness) for the crack parameters was taken, namely:

$$J = \alpha\sigma_0\ \varepsilon_0\ b\ h_1(a/W,n)\ (P/P_0)^{n+1} \tag{17}$$

$$\delta = \alpha\varepsilon_0\ a\ h_2(a/W,n)\ (P/P_0)^n \tag{18}$$

where J is the applied J-Integral, and δ, the crack opening displacement at the edge of the specimen, a/W is the dimensionless crack length, W the specimen width, b, the ligament (W-a) and P_0 the limiting load, given as:

$$P_0 = 0.728\ \sigma_0\ b^2/L$$

with L, the specimen half-length. The two polynomials h_1 and h_2 thus represent the normalized J-Integral and CMOD respectively. Their value depends only on the crack length and on the hardening index. Results obtained in this study are presented in Fig. 3. As can be seen, correlation with the analysis of Kumar et al. (1981b) is generally good, the error being within 5%. The procedure used for computing J is described below. The program was run in double-precision on a 3090 IBM mainframe. Four iterations, complete with tangent matrix evaluation and displacement solution, were typically accomplished within one cpu minute. The FEM grid contained 29 substructures, 2872 DOF before reduction, and 920 DOF in the reduced state.

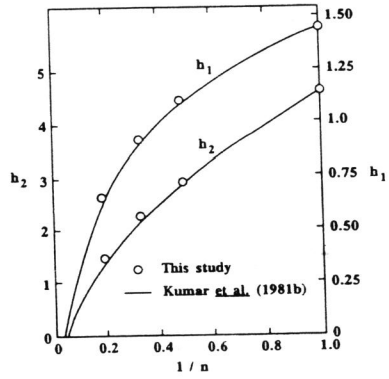

Fig. 3 Normalized J-Integral, h_1 and crack mouth displacement, h_2 for a single-edge cracked plate under three-point bending (a/W = 0.6)

The J-Integral was computed from the virtual crack extension method due to Parks. In the incompressible state and for CST elements, the following was used:

$$J = \sum_e A_e \left(S_1 \frac{\partial\varepsilon_1}{\partial a} + S_2 \frac{\partial\varepsilon_2}{\partial a} + S_3 \frac{\partial\varepsilon_3}{\partial a}\right) + \Phi\left|\frac{\partial A_e}{\partial a}\right| \tag{19}$$

in which derivations are approximated by:

$$\frac{\partial f}{\partial a} \simeq \frac{1}{\Delta a}\left(f(a+\Delta a) - f(a)\right)$$

A_e is the surface of element e, Δa, the virtual crack advance, and Φ the plastic strain energy density, given as:

$$\Phi = \frac{c\ n}{n+1}\ \varepsilon_e^{(n+1)/n} \qquad (20)$$

Rings of 40 elements were considered in the above summation. The criterion was found insensitive to node shift Δa of the interior contour in the range 10^{-8} to 10^{-4} (for a = 3 and W = 5). Computations were currently done with 20 rings, the first one being r_0, the crack tip radius itself. Consistant results were generally found starting from the 4th ring, located at distance 0.003 W from the crack tip.

DETERMINATION OF THE HYDROSTATIC STRESS

Once a convergent solution was obtained for the displacements, the incompressibility of the strain components was checked in order to validate the quality of the solution, and the hydrostatic stress was computed.

The hydrostatic stress (one per element) was introduced as a Lagrange multiplier in the FEM formulation. This is an alternative for the formulation of the same problem. In discretized form, for a given substructure:

$$[K]\{u_i\} + [C]^T\{\sigma_h\} = \{F_i\} \qquad (21)$$

in which [K] is the stiffness matrix of the unconstrained system, [C], the incompressibility constraints, as given by Eq. (7), σ_h, the hydrostatic stress, and $\{F_i\}$, the nodal forces. Equation (21) can be written:

$$[C][C]^T\{\sigma_h\} = [C]\left\{\{F_i\} - [K]\{u_i\}\right\}$$

where $[C][C]^T$ is a square (8N x 8N) matrix. LU triangular factorisation was used to solve this relatively small system. Triangular matrices were profiled using the sky-line method. An example of normal stress plot ($\sigma_2 = S_2+\sigma_h$) is illustrated in Fig. 4 for a double-edge notched plate under remote tension, $\sigma^\infty = 10.4$.

CONCLUDING REMARKS

Used in conjunction with LEFM solutions, the fully plastic solutions obtained from the program developed in this study yield directly to a complete elastic-plastic solution and to the construction of crack driving force diagrams for structural integrity assessment. Various planar and axi-symmetric geometries can be "calibrated" efficiently using this method. A large variety of ductile steels and non-ferrous alloys can be described with the single pure-law hardening stress-strain relation. Combinations of a power-law at a given strain hardening index with others at different exponents are also possible for materials exhibiting variable strain-hardening rate.

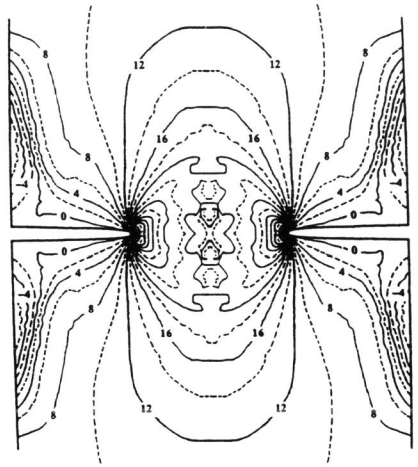

Fig. 4. Normal stress lines in a double-edge notched plate (solution for n = 3, $\sigma^\infty = 10.4$)

REFERENCES

Goldman, N.L. and J.W. Hutchison (1975). Fully plastic crack problems: the center-cracked strip under plane strain. Int. J. Solids Structures, 11, 575-591.

Kumar, V., M.D. German and C.F. Shih (1981a). Elastic-plastic and fully plastic analysis of crack initiation, stable growth and instability in flawed cylinders. In: Elastic-Plastic Fracture (Shih/Gudas, ed.), Vol. I, pp. 306-353. ASTM STP 803, Philadelphia.

Kumar, V., M.D. German and C.F. Shih (1981b). An engineering approach for elastic-plastic fracture analysis. Electrical Power Research Institute (EPRI NP-1931), project 1237-1.

Nagtegaal, J.C., D.M. Parks and J.R. Rice (1974). On numerically accurate finite element solutions in the fully plastic range. Comp. Meth. in App. Mech. and Eng., 4, 153-177.

Needleman, A. and C.F. Shih (1978). A finite element method for plane strain deformations of incompressible solids. Comp. Meth. in App. Mech. and Eng., 15, 223-240.

Zienkiewicz, O.C. (1977a). Constrained variational principles. Penalty functions and the least square method. In: The Finite Element Method (third edition), Chap. 3, pp. 83-89. McGraw-Hill Book Company, London.

Zienwiewicz, O.C. (1977b). Constrained variational principles. Lagrange Multipliers and Adjoint functions. In: The Finite Element Method (third edition), Chap. 3, pp. 77-83. McGraw-Hill Book Company, London.